

Article www.acsanm.org

# Activated Carbon-Metal Organic Framework Composite for the Adsorption of Contaminants of Emerging Concern from Water

Juan C. Muñoz-Senmache, Sewoon Kim, Rodinson R. Arrieta-Pérez, Chang Min Park, Yeomin Yoon, and Arturo J. Hernández-Maldonado\*



Cite This: ACS Appl. Nano Mater. 2020, 3, 2928-2940



**ACCESS** I

Metrics & More

Article Recommendations

Supporting Information

ABSTRACT: A composite adsorbent (CMOF) based on in situ growth of MIL-100Fe (MOF) within the macro- and mesopores of a Darco-KB-G activated carbon (AC) was prepared for the efficient adsorption of a set of contaminants of emerging concern (CECs), namely, caffeine (CFN), carbamazepine (CBZ), clofibric acid (CA), 10,11-epoxycarbamazepine (Ep-CBZ), naproxen (NPX), o-desmethylnaproxen (o-DMN), paraxanthine (PXN), and salicylic acid (SA), from water. The properties of the composite and that of the parent materials were evaluated via X-ray diffraction, scanning electron microscopy, nitrogen porosimetry, thermal gravimetric analysis (TGA), and X-ray photoelectron microscopy. Mass



balances indicate that the composite contains about 46 wt % MOF, while a comparison of pore size distributions and TGA corroborated that the vast majority of the crystalline material resides within the macro/mesopores of the AC. Zeta potential measurements revealed that the acid media used during the in situ growth of the MOF resulted in a CMOF surface charge profile (isoelectric point (IEP) =  $\sim$ 3.2) that is generally more negative than that of the MIL-100(Fe) (IEP =  $\sim$ 4.2) and the nonacid treated AC (IEP =  $\sim$ 5.5). Single and multicomponent CEC equilibrium adsorption tests were performed at room temperature, neutral pH conditions, and low CEC concentrations (~µg L<sup>-1</sup>). Single component adsorption data show that the composite adsorbs 10-fold more CEC molecules compared to the MOF alone, with a selectivity that increases as follows: CA < SA < o-DMN < PXN < NPX < CFN < Ep-CBZ < CBZ. The effect of competition among the CECs on the adsorption capacity of CMOF was not as significant, only about 9% smaller compared to single component adsorption data. Uptake improvements seen in the CMOF appear to be the result of interactions based on a combination of hydrophobicity (from the AC core) and enhanced electrostatic level forces as well as  $\pi$ -complexation and  $\pi$ - $\pi$  stacking interactions.

KEYWORDS: metal organic framework, composite adsorbent, in situ crystal growth, contaminants of emerging concern, water remediation

# 1. INTRODUCTION

The constant increase in global population and, therefore, demand for high quality water supply are bringing significant scientific and engineering challenges to society. Challenges include the scarcity of water resources due to intensifications of droughts, which have already triggered the adoption policies to allow for more usage of reclaimed water, especially in arid or semiarid regions, in order to reduce possible impacts on activities such as agriculture. 1-3 For example, the state of California (USA) has predicted an increase of about 40% in the use of reclaimed water by 2020 and almost 3-fold more (280%) by 2030.4 Further complications will arise due to the ever increasing concentrations of contaminants of emerging concern (CECs) in water streams as a direct result of human activities. These contaminants include pharmaceuticals, pesticides, endocrine disrupting agents, and metabolites, just to mention a few.<sup>5-8</sup> For example, the use of reclaimed water and the intrinsic ability of plants to uptake compounds from the soil and/or water have led to a number of reports on how CECs are now present in food crops (e.g., roots, tubers, and/or

vegetables) $^{9-12}$  in amounts that could be toxic to human beings. $^{13-15}$ 

Around the globe, several wastewater treatment plants (WWTP) are already implementing strategies to remove CECs. Examples include those found in Switzerland and Germany. The former is result of legislation to implement technical measures in WWTPs to address removal of CECs while for the latter the implementation is carried out on a voluntary basis. 16,17 Due to the diversity of physical and chemical properties, the effective removal of CECs requires a combination of complementary processes to achieve effective and efficient removal from water. These could include conventional secondary treatments (e.g., activated sludge

Received: January 22, 2020 Accepted: February 18, 2020 Published: February 18, 2020



Scheme 1. Synthesis of CMOF Composite Adsorbent for the Removal of CECs

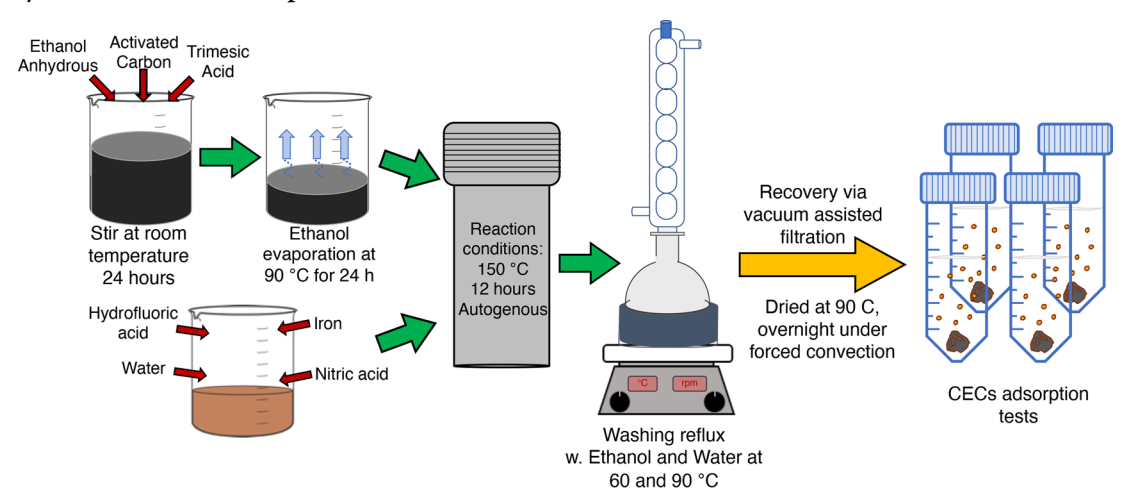


Table 1. Physicochemical Properties of Selected CECs

CEC	Description	pK <sub>a</sub> <sup>a</sup>	Log K <sub>ow</sub> <sup>a</sup>	Melting Point (°C)	Chemical structure <sup>a</sup>
Caffeine (CFN)	Nervous stimulant	14.00/ 0.60	-0.07	238	H <sub>b</sub> C CH <sub>b</sub>
Carbamazepine (CBZ)	Antiepileptic	13.94	1.89	204	HAN
Clofibric acid (CA)	Lipid regulator, herbicide	3.18	-0.99	120	H <sub>B</sub> C CH <sub>B</sub>
10,11 - Epoxy- carbamazepine (Ep-CBZ)	CBZ metabolite	N/A	1.97	212	N.N.
Naproxen (NPX)	Analgesic and anti- inflammatory	4.20	2.84	153	OH 0
o-Desmethyl- naproxen (o-DMN)	NPX metabolite	4.34/ 9.78	3.9	185	HO CH <sub>1</sub>
Paraxanthine (PXN)	CFN metabolite	10.76	-0.39	300	H <sub>3</sub> C CH <sub>3</sub>
Salicylic acid (SA)	Acetylsalicylic acid metabolite; analge- sic and anti- inflammatory	2.97	1.98	158	OH

 $<sup>^</sup>a$ Chemical structure and p $K_{\rm a}$  and log  $K_{\rm ow}$  values where gathered from literature reports.  $^{34,59}$ 

process) and tertiary treatments<sup>8,17,18</sup> such as advanced oxidation processes (i.e., ozonation, Fenton oxidation, ultraviolet treatment, and/or ionizing irradiation),<sup>17,19</sup> membrane filtration,<sup>20</sup> biodegradation,<sup>21</sup> and/or adsorption pro-

cesses.<sup>22–24</sup> Adsorption processes, which serve as the basis for this work, offer the potential of developing a separation strategy of low energy consumption, relatively low operational

costs, ease of implementation, and remediation without toxic byproducts.<sup>23</sup>

Various porous materials have been modified and tested as potential adsorbents of CECs, the former with emphasis on increasing selectivity and capacity. Examples of these materials include carbons, <sup>25–28</sup> zeolites, <sup>29–32</sup> clays, <sup>32,33</sup> silicas, <sup>34–36</sup> and metal organic frameworks (MOFs). <sup>23,24,37–39</sup> Among the carbon family, activated carbons adsorbents are commonly used for the adsorption of organic compounds due to their large porosity, hydrophobicity, and relative low cost; however, the irregularity of the distribution of its pore size and weak adsorbate-adsorbent surface interactions bring disadvantages, when processing water with a complex matrix of contaminants. 40 MOF adsorbents offer superior surface area, welldefined, uniform porous structures, and flexible surface tailoring capabilities to control selectivity, 38,41,42 but hydrophobicity results in less than ideal adsorption working capacities. Among the MOFs used for adsorption from aqueous media, MIL-100(Fe) is one of the most prom-It consists of a three-dimensional structure composed of iron nodes and trimesic acid as linkers, and that showcases large surface area and pore volume (1350-2300 m<sup>2</sup> g<sup>-1</sup> and 0.82-1.20 cm<sup>3</sup> g<sup>-1</sup>, respectively); the porosity is characterized by two large cages (25 and 29 Å) that are accessible via windows of 5 and 9 Å in diameter. 48-51 The latter are sufficiently large to allow passage of various CEC types, while allowing for size exclusion of larger molecules that might compete for adsorption sites during water treatment. MIL-100(Fe) also offers sites that might selectively interact with adsorbates based on nonspecific electrostatic interactions and/or complexation (through the metal nodes), providing other mechanisms for the selective adsorption of CECs that contain similar physical characteristics. Previous studies performed by Hernandez-Maldonado and co-workers for the removal of CECs using different adsorbent classes containing transition metals acting as sites for interactions with adsorbates have shown that complexation plays an important role. 29,34,52,53 It is hypothesized that the same could take place in MOFs such as MIL-100(Fe). Furthermore, a composite material based on activated carbon and MIL-100(Fe) might result in a promising platform to develop an effective CEC adsorbent based on a synergistic combination of the advantages and properties of each constituent in the composite.

The objective of this work is to synthesize, characterize, and test a composite (CMOF) based on the in situ growth of MIL-100(Fe) within the macro- and mesopores of activated carbon (Darco KB-G) for the adsorption of a particular set of CECs from water (Scheme 1). The CECs used in this study (i.e., caffeine (CFN), carbamazepine (CBZ), clofibric acid (CA), 10,11-epoxycarbamazepine (Ep-CBZ), naproxen (NPX), odesmethylnaproxen (o-DMN), paraxanthine (PXN), and salicylic acid (SA)) were selected to include both source and metabolite contaminants, while also ensuring a variety of physical and chemical properties (i.e., size, acid dissociation constant  $pK_a$ , and partition coefficient  $K_{OW}$ ) (see Table 1).

# 2. EXPERIMENTAL SECTION

**2.1. Reagents and Materials.** For the synthesis of MIL-100(Fe) and composite, the materials used were iron chips, trimesic acid (H<sub>3</sub>BTC), nitric acid, hydrofluoric acid, ammonium acetate, ethanol, and methanol. All of these were obtained from Sigma-Aldrich (USA) and used as received. The activated carbon (Darko KB-G, AC) was

obtained from Sigma-Aldrich (USA), and the required deionized water (18  $M\Omega$  cm) was produced in house.

Caffeine (CFN), carbamazepine (CBZ), clofibric acid (CA), 10,11-epoxycarbamazepine (Ep-CBZ), naproxen (NPX), o-desmethylnaproxen (o-DMN), paraxanthine (PXN), and salicylic acid (SA) were all obtained from Sigma-Aldrich (USA) and used as received. All the reagents employed during liquid chromatography—mass spectroscopy tests were acetonitrile, water, ammonium acetate, methanol, and formic acid. These were all obtained from Honeywell (USA) and Agilent (USA).

Ultrahigh-purity grade  $N_2$  (Praxair, Inc.) was used for determination of textural properties as well as a carrier gas during thermogravimetric analyses (TGA). High-purity grade He gas (Praxair, Inc.) was used as a backfill gas during the adsorbent activation and prior to the  $N_2$  adsorption tests.

**2.2. Synthesis of MIL-100Fe (MOF).** MIL-100(Fe) was prepared based on recipes available elsewhere. 43,48,49 However, some modifications were applied to ensure that the structure of the MOF would withstand a range of pH during the CECs adsorption tests. Bezverkhyy et al. found that the structural stability of iron-containing MOFs, including MIL-100(Fe), that were synthesized under fluoridefree conditions are severely degraded when these materials are exposed to water, and the pH was brought to neutral using buffer solutions.<sup>54</sup> Therefore, for the present study, a solution with the following composition 1.0 Fe:0.66 H<sub>2</sub>BTC:2.0 HF:1.2 HNO<sub>2</sub>:280 H<sub>2</sub>O was mixed in a Teflon lined reactor and heated to 150 °C for 12 h (Scheme 1). Upon cooling to room temperature, the solution was vacuum filtered to yield a light-orange colored solid product. For the removal of excess compounds (e.g., trimesic acid, nitric acid, hydrofluoric acid, and/or iron), the recovered solids were washed under reflux first using deionized water at 85 °C for 5 h and then using ethanol at 65 °C for 3 h. Finally, the remaining solid product was dried at 90 °C overnight in a forced convection oven. A yield of about 50% was achieved.

2.3. Synthesis of MIL-100Fe/Activated Carbon Composite (CMOF). The synthesis of CMOF was carried out in two stages. The first consists of the dispersion of trimesic acid onto AC. A trimesic acid ethanol solution (about 1 g of trimesic acid per 10 g of ethanol<sup>55</sup>) was prepared and later dispersed onto AC (about 10 g of solution per 0.6 g of AC). The amount of solution that was dispersed was determined based on the MIL-100(Fe) synthesis yield and complete occupancy of the macro- and mesopore total pore volume of AC as estimated from porosimetry analyses (refer to the materials characterization description below). The acid/carbon mixture was then placed in a forced convection oven at 90 °C for 24 h to evaporate the ethanol. The second stage was the addition of the rest of the reactants necessary to produce crystals of MIL-100(Fe) according to the composition and conditions presented in the previous section.

Given that the surface of AC was exposed to acid treatment (i.e., H<sub>3</sub>BTC, HF, and HNO<sub>3</sub>) at some point during the preparation of CMOF, the resulting carbon (AC-AT) was considered for the CEC adsorption tests to elucidate the effect that such treatment might have on the surface of the material and hence the adsorption mechanism. AC-AT was prepared by treating the as-received Darko KB-G activated carbon solely with the aforementioned acids.

**2.4. Materials Characterization.** Identification of the periodic phase of the synthesized materials was accomplished via powder X-ray diffraction (XRD). The data were collected using a Rigaku UTIMA III X-ray diffractometer fitted with a Cu K $\alpha$  anode ( $\lambda$  = 1.5418 Å). The anode was operated at 40 kV and 44 mA, and the patterns were gathered between the 2° and 20° 2 $\theta$  range at a scanning speed of 0.5° min<sup>-1</sup>. To verify for the structural stability of MIL-100(Fe) and CMOF after uptake of CECs, the adsorbents were first recovered by centrifugation, then dried overnight (at conditions to be determined by thermal gravimetric analyses), and then tested for crystallinity/integrity also using XRD.

The morphology of the adsorbents and their corresponding elemental composition were observed using a scanning electron

Table 2. Selected Textural Properties of Different Adsorbent Materials

material	BET total area <sup>a</sup> (m <sup>2</sup> cm <sup>-3</sup> )	total pore volume <sup>a</sup> (cm <sup>3</sup> cm <sup>-3</sup> )	micropore volume <sup>b</sup> (cm <sup>3</sup> cm <sup>-3</sup> )	average pore size $^b$ (Å)	density (g cm <sup>-3</sup> )
MIL-100(Fe) MOF	1110	0.62	0.55	5.0, 8.6, 24.8	0.70
activated carbon	380	0.40	0.03	5.0-6.0, 7.5-8.5, >50	0.31
activated carbon after acid treatment	197	0.14	0.14	5	0.31
MIL-100((Fe) activated carbon composite (CMOF)	815	0.72	0.43	4.9, 8.4, 24.3	0.60

<sup>a</sup>From N<sub>2</sub> equilibrium adsorption gathered at -196 °C. <sup>b</sup>Estimated via the Horvath-Kawasoe method.

microscopy (SEM) in a Hitachi-SU8230 microscope also equipped with an energy-dispersive X-ray (EDAX) attachment.

Thermogravimetric analyses (TGA) were performed using a high-resolution TA Instruments D550 unit while operating with a constant gas flow of  $N_2$  and air at 60 mL min<sup>-1</sup>. Each material (i.e., MIL-100(Fe), CMOF, and AC-AT) was heated from room temperature to 700 °C at a rate of 10 °C min<sup>-1</sup> and kept at 700 °C for 30 min (i.e., ramp and soak). TGA analyses allowed determination of the temperature at which each structure might collapse, the amount of water adsorbed or coordinated to each material, and also decomposition pathways. TGA data was also used for determination of the overall chemical composition of the MOF phase as well as to elucidate regeneration options for spent adsorbents based on thermal purging and reactivation.

Textural properties were estimated via N2 equilibrium adsorption isotherms gathered at −196 °C (77 K). The data were collected using a Micromeritics ASAP 2020 volumetric adsorption instrument fitted with turbomolecular drag pumps. Prior to each nitrogen adsorption measurement, the as-synthesized MIL-100(Fe) was degassed in vacuum at 120 °C for 12 h, while AC, AC-AT, and CMOF were degassed at 150 °C for 16 h. These temperatures were determined based TGA tests as indicated above. Nitrogen adsorption-desorption amounts were normalized by volume of the adsorbent particle instead of mass to account for significant differences in density among the materials. The BET (Brunauer, Emmett, and Teller) isotherm model<sup>56</sup> was used to determine the surface area, the Barrett-Joyner-Halenda<sup>57</sup> (BJH) model was used to calculate the pore volume and the mesopore size distribution, and the Horvath-Kawazoe approach (as corrected by Yang and co-workers)<sup>58</sup> was used to determine the micropore size distribution.

X-ray photoelectron spectroscopy measurements were developed using a PHI Versa Probe (II) 5000 unit with monochromatized Al K $\alpha$  radiation ( $h\nu$  = 1486.6 eV), and C 1s (284.5 eV) was used to calibrate the binding energies. The pass energy used for the high-resolution elemental spectra was 46.95 eV.

Zeta potential measurements were used to determine the behavior of the adsorbents surface charge as a function of pH. Brookhaven ZetaPals equipment was used. In a typical test, the materials were suspended in water (0.50% wt) and the data was collected in the  $3-10~\rm pH$  range; the ionic strength was maintained during tests using a 1 mM KCl solution.

2.5. Kinetic and Equilibrium Adsorption Experiments. A transient adsorption test was used to estimate the time required to reach equilibrium conditions and to estimate diffusion coefficients. Carbamazepine was chosen for this part since it is among the largest CEC molecules used in this study and it also remains neutrally charged in aqueous solutions. About 10 mg of each adsorbent and 10 mL (for MIL-100(Fe) and CMOF and 30 mL for AC-AT) of a 100  $\mu g L^{-1}$  CBZ solution were mixed in borosilicate centrifuge tubes and shaken at 200 rpm for specific time intervals at room temperature. The samples were centrifuged at 8500 rpm for at least 5 min, and the supernatant was filtered using 0.2  $\mu$ m PTFE discs. The carbamazepine concentration in the liquid was determined using an Agilent 1290 high- performance liquid chromatography system coupled to a 6460 triple quadrupole mass spectrometer (HPLC-MS/MS) fitted with an Agilent Zorbax Eclipse Plus C18 (2.1 mm × 50 mm and particle size 1.8  $\mu$ m) column that was operated at 40 °C. The MS system also included an Agilent Jet Stream electrospray ionization (AJS-ESI) with multiple reaction monitoring (MRM) setup. The adsorbed amount of the CEC (i.e., carbamazepine) was estimated via a mass balance:

$$q(t) = \frac{[C_0 - C(t)]V_{\text{solution}}}{V_{\text{adsorbent}}} \times 10^3$$
 (1)

where q(t) is the adsorbed amount ( $\mu g$  cm<sup>-3</sup>),  $C_0$  is the initial concentration of the CEC in solution, and C(t) is the concentration of the CEC in solution at any time t, both expressed in  $\mu g$  L<sup>-1</sup>,  $V_{\text{solution}}$  is the total liquid volume of CEC solution (L), and  $V_{\text{adsorbent}}$  is the solid volume of the adsorbent (cm<sup>3</sup>).

CEC equilibrium adsorption experiments (single- and multicomponent) for each material (MOF, AC-AT, and CMOF) were performed by mixing 10 mL of the target CEC solution with 10 mg of adsorbent at room temperature for 24 h. The pH of the initial solution, which changed spontaneously depending on the adsorbent material, was adjusted using sodium hydroxide 0.1 M to obtain a neutral pH (6.5–7.5) at equilibrium conditions. Triplicate measurements were performed, and the determination of the equilibrium concentration was calculated using the HPLC–MS/MS system described above. Adsorbed amounts were calculated also with eq 1 at t=24 h. The resulting isotherm data were fitted using the Freundlich and Sips models:

$$q = K_{\rm F} C_{\rm e}^{1/n_{\rm F}} \tag{2}$$

$$q = \frac{q_{\text{sat}} K_{\text{S}} C_{\text{e}}^{1/n_{\text{S}}}}{1 + K_{\text{S}} C_{\text{e}}^{1/n_{\text{S}}}}$$
(3)

where q is the adsorbed amount ( $\mu g$  cm<sup>-3</sup>) at a specific equilibrium concentration,  $C_e$  ( $\mu g$  L<sup>-1</sup>),  $K_F$  and  $K_S$  are the interaction parameters (subscripts F for Freundlich and S for Sips),  $n_F$  or  $n_S$  is a qualitative indicator of the adsorbent material surface heterogeneity, and  $q_m$  is the CEC maximum adsorbed amount ( $\mu g$  cm<sup>-3</sup>). All the CEC adsorption amounts were normalized by volume of adsorbent instead of weight since, in the case of the CMOF composite, the MOF contained inside of AC generates heterogeneity in bulk density and, hence, comparing the performance of each adsorbent with respect to volume is more accurate. The density was calculated under the assumption that the macro- and mesopores of activated carbon are filled with MOF (see Table 2).

**2.6. Recyclability of CMOF.** The recyclability of the CMOF adsorbent was evaluated based on a three cycle tests for uptake of carbamazepine (CBZ). For each cycle, 40 mg of adsorbent and 40 mL of CBZ solution at 200  $\mu$ g L<sup>-1</sup> were mixed in a centrifuge tube and shaken at room temperature for 6 h. The pH was adjusted using NaOH 0.1 M to obtain neutral pH. After each cycle of adsorption, the material was recovered via centrifugation and then dried using flow air (100 mL min<sup>-1</sup>) at 35 °C overnight, then heated at 25 C h<sup>-1</sup> until 205 °C and kept for 12 h in air flow (100 mL min<sup>-1</sup>). The obtained material was then used for the next adsorption cycle. The percent of removal was calculated as follows:

$$\% \text{ removal} = \frac{C_i - C_f}{C_i} \times 100\%$$
(4)

where  $C_i$  and  $C_f$  are the initial and final concentrations of CBZ in the solution, respectively. To evaluate the structural stability of the

CMOF adsorbent, XRD patterns were taken prior to each adsorption cycle.

# 3. RESULTS AND DISCUSSION

**3.1. Structural and Textural Analysis.** The crystallinity of MIL-100(Fe) MOF and the corresponding periodic phase of the CMOF were corroborated via XRD. The profiles shown in Figure 1 are in agreement with literature data reported

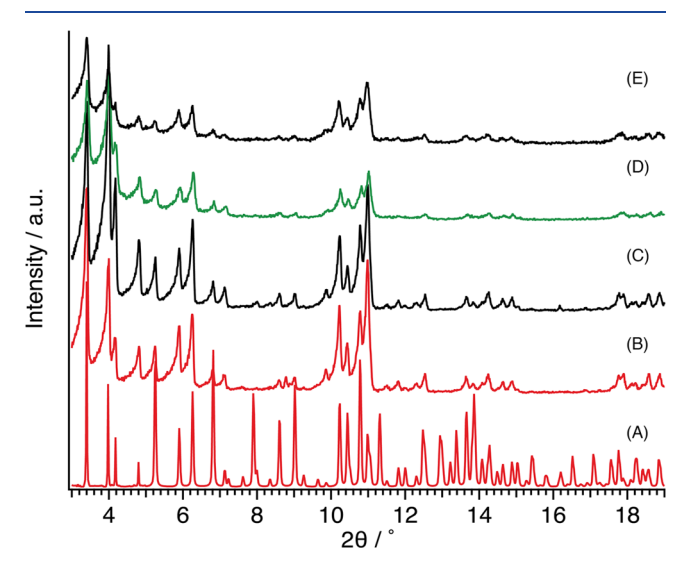


**Figure 1.** (A) Simulated and (B–E) experimental X-ray diffraction patterns for (A and B) MIL-100(Fe) (MOF), (D) MIL-100(Fe)/ activated composite (CMOF), and spent (C) MOF and (E) CMOF.

elsewhere for the general phase order of MIL-100(Fe).  $^{42,48}$  The relative decrease in intensity observed in the CMOF diffraction profile could be ascribed to deconstructive scattering caused by the AC (i.e., amorphous phase); however, the reflections typical of the MOF periodicity that is located at  $2\theta$  3.4, 4.0, 10.2, 10.5, 10.8, and  $11.0^{\circ}$  remained visible in the CMOF material XRD pattern. These peaks correspond to diffraction planes that intersect the main pore window perimeter and the super cage of the MOF structure.

The morphology of the materials was observed using SEM, and the resulting micrographs are shown in Figure 2. As expected, the activated carbon consisted of an amorphous phase (Figure 2A), and this was not affected by acidic treatment (Figure 2B). MIL-100Fe phase consists of octahedrally shaped crystals<sup>60,61</sup> with sizes of about ~200-300 nm (Figure 2C). Meanwhile, Figure 2D shows that the morphology of the activated carbon prevails in the CMOF adsorbent, although small amounts of MIL-100(Fe) were also observed outside of activated carbon. However, elemental compositional mapping via EDAX revealed the presence of iron and fluorine (both constituents of the MIL-100(Fe) structure) throughout all the composite (Figure 2E,F, respectively). This offers strong evidence that most of the MOF phase grew within the void space of the pores of the carbon phase. It should be noted that similar observations have been made in other metal organic framework/porous carbon composites reported elsewhere. 62,63

Figure S2 shows nitrogen adsorption—desorption isotherms that were gathered for MIL-100(Fe), AC, AC-AT, or CMOF at -196 °C. The adsorbed amounts shown in the ordinate are normalized by volume of adsorbent instead of weight, since the MOF contained inside of AC creates heterogeneity in bulk

density; hence, comparing the performance of each adsorbent with respect to volume is more accurate. In addition, the adsorbent density was calculated under the assumption that the mesopores of activated carbon are filled with MOF and, as will be shown later, this assumption was verified via pore size distribution (PSD) and TGA tests. Values of surface area, pore volumes, and density are shown in Table 2.

The N<sub>2</sub> isotherm profile observed for the MIL-100 (Fe) MOF is an intermediate between types I and IV as defined by IUPAC (International Union of Pure and Applied Chemistry). The increase in nitrogen adsorbed amounts between 0.01–0.05 and 0.10–0.16 relative pressure is due the presence of microporous windows and mesoporous cages; the former gives access to the latter. Nitrogen adsorption onto AC is, as expected, characteristic of a mesoporous and macroporous material (type IV) with a desorption hysteresis due to capillary condensation. The CMOF isotherm shows a type I/IV hybrid form with a smaller hysteresis gap compared to AC. Meanwhile, the effect of the exposing AC to acid is apparent in the textural properties; decreases in the total surface area, total pore volume, and loss of the mesoporosity and macroporosity were observed (Table 2).

PSD profiles are shown in Figure 3. A Horvath-Kawasoe analysis indicated that the micropores in MOF are 5.0 and 8.6 Å in diameter, which agrees well with reports available elsewhere. 43,49 AC shows a range of micropore diameters (i.e., 5.0-6.0 Å and 7.5-8.5 Å) besides the expected mesopore dimensions. However, upon acid treatment, the AC bimodal PSD is no longer visible. Instead, a single pore diameter of 5 Å is estimated probably due to destruction and reconfiguration of the AC carbon surface. In the case of the CMOF material, the diameter and volume of micropores that correspond to the MOF decreased (Table 2), which is reasonable since the MOF represents just a fraction of the overall composition of the composite. The micropores section of the CMOF PSD that corresponds to the activated carbon disappeared, probably due to in situ growth of the MOF which will effectively block access of N<sub>2</sub> to the micropores. The changes observed in the textural properties of the AC but not in the CMOF after the acid treatment are probably due to the presence of MOF on the latter, which serves as a protective layer to the surface of the AC in the composite. The acidic treatment affects the porosity of the AC probably because of reactions happening on the surface (i.e., oxidation of functional groups).

TGA decomposition profiles under a nitrogen atmosphere and corresponding differential plots are shown in Figure 4; profiles under an air atmosphere are shown in Figure S3. The TGA profile of MIL-100(Fe) (i.e., MOF) matches well with the data obtained by Horcajada et al.;<sup>48</sup> there are three weight loss regions corresponding to the elimination of physisorbed water (~75 °C), water coordinated to the iron trimers (100-270 °C), and the ligands based on the trimesic acid (~420 °C). The remaining mass corresponds to iron oxide or an iron complex. The decomposition profiles for AC and AC-AT show elimination of physisorbed water, with a weight loss region located near the 100 °C mark. A second weight loss corresponding to the evacuation of surface functional groups (i.e., -CHO, -OH, -CO) was observed at ~250 °C, and a final weight loss corresponding to the pyrolysis of the carbon was observed at  $\sim$ 450  $^{\circ}$ C. In the case of the CMOF, the TGA profile also shows most of the previously mentioned weight loss features plus the decomposition section corresponding to the pyrolysis of the activated carbon. A reduction of ~18% in

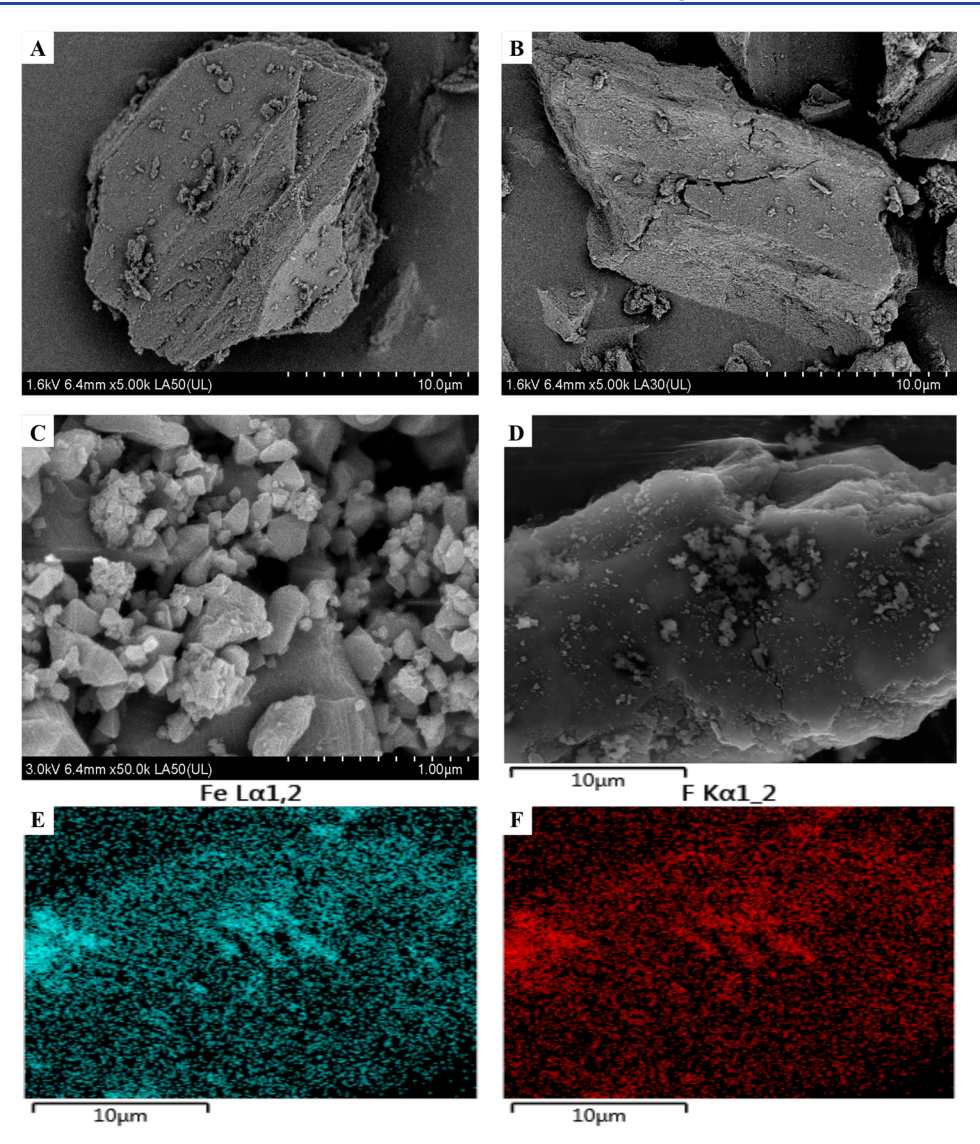
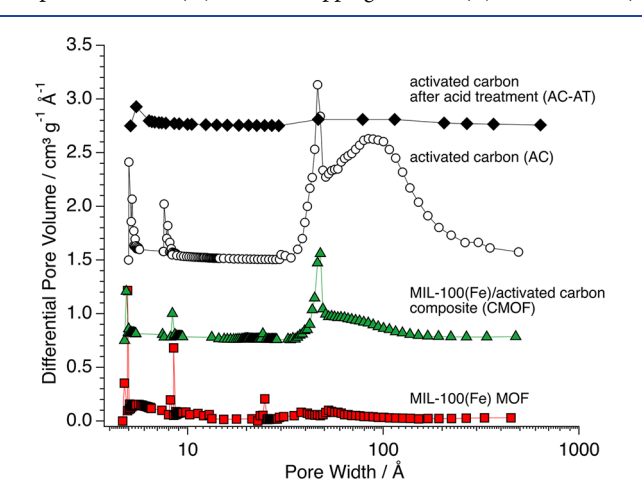


Figure 2. SEM images of activated carbon (A), activated carbon treated with acid (B), MIL-100(Fe) (C), and MIL-100(Fe)/activated carbon composite CMOF (D). EDAX mapping for iron (E) and fluorine (F) in the same perimeter area shown in part D.



**Figure 3.** Pore size distribution estimated using the corrected Horvath–Kawasoe adsorption and BJH desorption methods.

physisorbed water content was observed relative to the assynthesized MOF. Interestingly, the profile or the corresponding differential plot shows no evidence of any coordinated water, and this might be due to the hydrophobicity of the activated carbon core. The next weight loss region corresponds to the decomposition of functional groups of the AC-AT core as well as the trimesic acid ligands. The latter decomposition takes place at a higher temperature range compared to that of the MOF; although the ligand decomposition follows a stepwise degradation path typical of an organic molecule that decomposes in the presence of a solid surface, the decomposition products in the CMOF need to desorb and diffuse along the carbon mesopores. This adds an energy barrier for the complete elimination of the volatile residues and hence the observed temperature range displacement observed in Figure 4. The average temperature required to decompose the ligand increased from ~420 to ~490 °C.

The amount of MOF present in CMOF can be elucidated upon combination of the textural, TGA, and mass balance analyses. As the basis for the calculation, the ratio of MOF ligands to iron trimers should remain constant during the preparation of the CMOF and, on an anhydrous basis, a mass balance using TGA data yields that the amount of MOF in the composite is about 46 wt %. This was also corroborated by comparison of residual amounts observed for AC, MOF, and

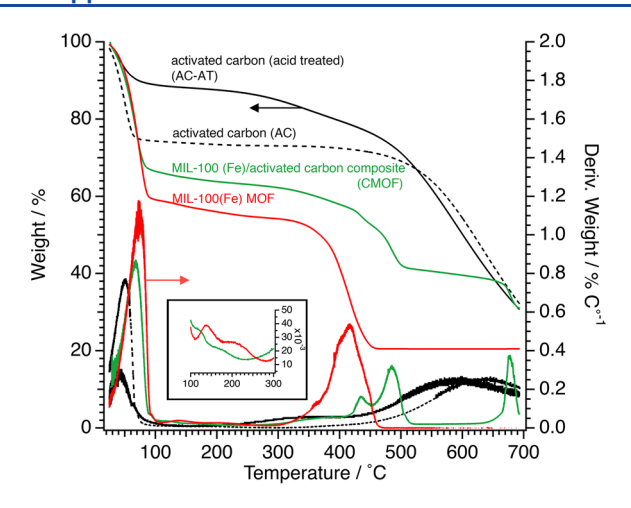


**Figure 4.** Thermal gravimetric analysis weight loss and derivative weight loss profiles for MIL-100(Fe) (MOF), activated carbon (AC), activated carbon after acid treatment (AC-AT), and MIL-100(Fe)/activated composite (CMOF). Inset shows magnified portions of the derivative weight loss profiles for MIL-100(Fe) (MOF) and MIL-100(Fe)/activated composite (CMOF) between 100 and 200 °C.

CMOF in TGA profiles gathered under an air atmosphere (see Figure S3). In the case of the MOF, this is also given by the reported material unit cell formula Fe<sub>3</sub>O(H<sub>2</sub>O<sub>2</sub>)<sub>2</sub>F·  $[C_6H_3(CO_2)_3]_{2}$ , which matches quite well with the composition distribution shown by the MOF TGA profile shown in Figure 4. Using the textural properties data shown in Table 2 as well as the composition distribution suggested by the CMOF TGA profile (i.e., Figure 4), the CMOF has a mesopore volume of 64 cm<sup>3</sup> per 100 g of composite and the MOF is occupying 66 cm<sup>3</sup> also per 100 g of composite. Given that the pore size distributions (Figure 3) show clear evidence that most of the mesoporous voids of the AC disappear during the inclusion of the MOF, it is assumed that the majority of the MOF resides within those mesopores. This is crucial to take advantage of the hydrophobicity of the carbon during the adsorption of CECs.

High-resolution XPS spectra for C 1s and O 1s in the activated carbon are shown in Figure S4A. A deconvolution of the C 1s spectrum showed the presence of carbon black (285 eV). The breadth peak centered at 287.9 eV represents the functional groups<sup>65</sup> (i.e., C-O, C=O, -CHO, -COOH); these functional groups are also confirmed by the deconvoluted peak of the O 1s spectrum at 533.1 eV. Meanwhile, the acidic treatment of the carbon apparently resulted in an increase in concentration of these functional groups, as evidenced by the deconvoluted peak (centered at 287.1 eV) from the C 1s spectrum (Figure S4B). The C 1s, O 1s, and Fe 2p spectra of MIL-100Fe are shown in Figure S4C. C 1s can be deconvoluted into three peaks; the peaks at 286.2 and 288.5 eV correspond to the phenyl and carboxyl groups, 66 respectively, and the peak at 285 eV represent C-C bonds and carbon on the surface. The peak centered at 531.9 eV in the O 1s spectrum can be attributed to the presence of Fe-O-C species. A deconvolution of the Fe 2p spectrum show the peaks corresponding to Fe 2p<sub>1/2</sub> and Fe 2p<sub>3/2</sub> at 725.7 and 712 eV, respectively. 60° Also, their satellite peaks are shown centered at 735.5 and 716.3 eV. Figure S4D shows the spectra for C 1s, O 1s, and Fe 2p in CMOF. The deconvoluted peaks of C 1s show chemical surfaces states similar to that of activated carbon treated with acid (peak at 287.3 eV) and

MIL-100Fe (peak at 290.2 eV); however, the area below the deconvoluted peaks is larger for the peak similar to AC-AT than peak from MIL-100Fe. Similarly, deconvolution of the O 1s spectrum shows peaks corresponding to activated carbon treated with acid (532.8 eV) and MIL-100Fe (531.7 eV). The slight shifts of the peaks could be attributed to weak interactions between the surfaces of activated carbon treated with acids and MIL-100Fe. Finally, the peaks corresponding to Fe  $2p_{1/2}$  and Fe  $2p_{3/2}$  were found at the same position of MIL-100Fe.

**3.2. Surface Charge.** Zeta potential measurements were performed for each material to estimate surface charge profiles as a function of pH; the data are shown in Figure 5. The data

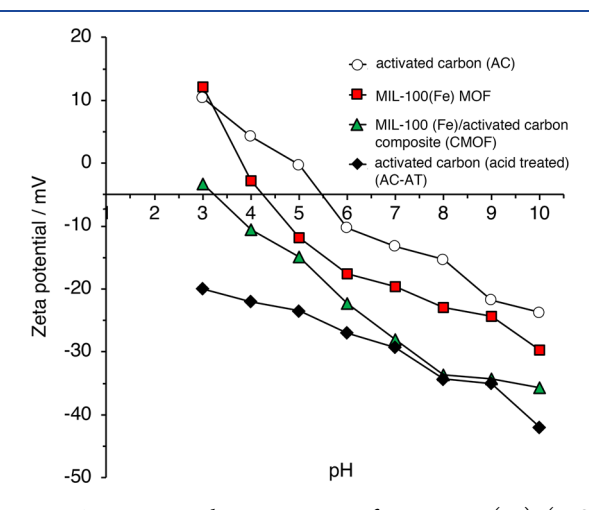


Figure 5. Zeta potential measurements for MIL-100(Fe) (MOF), activated carbon (AC), activated carbon after acid treatment (AC-AT), and MIL-100(Fe)/activated composite (CMOF).

for MOF and AC agrees with values reported elsewhere. <sup>29,43</sup> The acid treatment performed on AC (i.e., AC-AT) resulted in a negatively charged surface across the whole pH range. This explains why the CMOF surface charge profile is generally more negative than that of the MIL-100(Fe) and the nonacid treated AC, and these results are in agreement with the observations made from XPS measurements, where an increase in concentration of the surface carboxylic functional groups may transfer additional negative charges. Therefore, AC-AT and not AC was chosen for the CECs adsorption tests. The isoelectric point (IEP) for CMOF was  $\sim$ 3.2, and this value is smaller than that of the MIL-100(Fe) MOF ( $\sim$ 4.2).

**3.3. Single-Component CEC Equilibrium Adsorption.** According to the transient adsorption tests (see Figure S1), adsorption of CBZ onto CMOF and AC-AT reaches equilibration at  $\sim$ 10 min, while the equilibrium conditions for MOF takes  $\sim$ 2 h. The diffusion coefficients as estimated from a transport phenomenological model (see the Supporting Information) for CMOF, AC-AT, and MOF of 5.07  $\times$  10<sup>-16</sup>, 9.16  $\times$  10<sup>-15</sup>, and 1.86  $\times$  10<sup>-18</sup> m<sup>2</sup> s<sup>-1</sup>, respectively. These values reflect transport limitations due to steric effects (i.e., resistance due to pore dimensions), with the MOF representing an extreme given its microporous nature.

The adsorption equilibrium isotherms for each adsorbent material are shown in Figure 6, and these were gathered in both single and multicomponent adsorbate fashions, all at ambient temperature. Also, single point adsorption amounts at  $C_{\rm e} \sim 20~\mu{\rm g~L}^{-1}$  are shown in Figure S5 for comparison of total loading and selectivity among the adsorbents. All the adsorbed

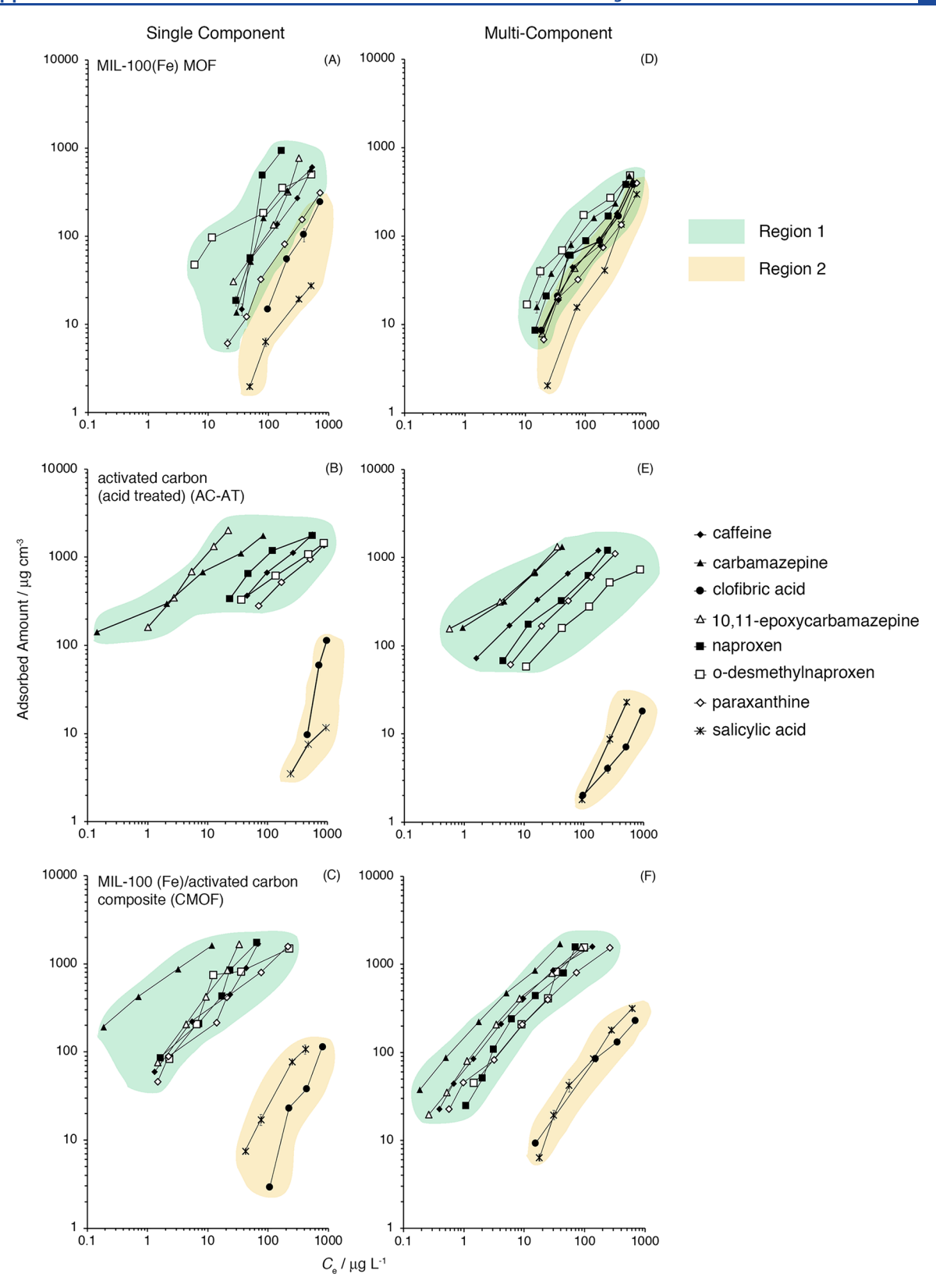


Figure 6. Adsorption equilibrium isotherms of CECs on (A and D) MIL-100(Fe) (MOF); (B and E) activated carbon after acid treatment (AC-AT), and (C) and (F) MIL-100(Fe)/activated composite (CMOF) materials. Parts A–C are for single-components, and parts D–F are for multicomponent adsorption data. Data was gathered at 25 °C and neutral pH.

amounts were normalized by the volume of adsorbent instead of the weight, this for reasons already explained above. Table S1 shows parameters for isotherm data fits with Freundlich and Sips models. Fit adequacy was evaluated with the residual root-

mean-square error (RRMSE). None of the adsorption measurements resulted in isotherm profiles that reached plateaus since the concentrations of CECs under consideration are not large enough to provide the necessary driving force to

achieve saturation; saturation adsorbed amounts ( $q_{\rm sat}$ ) were therefore estimated based on a pore filling mechanism and assuming that the adsorbates behave like hard spheres volumes that occupy all the available pore voids. Table S2 and Figures S6 and S7 show the resulting estimates for the fitting parameters and fit profiles, respectively.

As implied by the data shown in Figure 6A, for single component CEC adsorption, the overall affinity of MIL-100(Fe) toward CECs increases as follows: SA < CA < PXN < CFN < CBZ < Ep-CBZ < o-DMN  $\leq$  NPX. The good affinity toward NPX could be explained in terms of the hydrophobic nature ( $\log K_{ow} = 2.84$ ), which suppresses the anionic behavior  $(pK_a = 4.20)$  by weakening of the distribution of charges along its relatively large molecule size (~13.0 Å). In the case of o-DMN, the effect could be slightly decreased because the hydroxyl group placed in the ortho-position adds electronegativity. In contrast, the anionic behavior of SA dominates over hydrophobicity and, therefore, results in poor interactions with also the negative MOF surface. The slight increase in the adsorbed amount of Ep-CBZ over CBZ could be explained in terms of the difference of hydrophobic behavior (log  $K_{ow}$  = 1.97 vs 1.0, respectively), considering that both molecules remain without any charge at the prescribed pH. PXN has a slightly stronger hydrophilic behavior than CFN, and both molecules remain without any charges at neutral pH conditions. Furthermore, the methyl group that differentiates CFN from PXN brings a more electropositive behavior; these characteristics produce better interactions between CFN and MIL-100(Fe). Finally, the anionic and hydrophilic behavior of CA molecules (p $K_a$  = 3.18 and log  $K_{ow}$  = -0.99) led to weak adsorbent—adsorbate interactions. The slightly stronger interaction between SA and the adsorbent can be explained by the presence of electropositive methyl groups and the differences in the molecular dimensions of SA versus CA.

In the case of AC-AT (see Figure 6B), the adsorption isotherms can be segregated according to two distinct regions. Region 1 groups all the isotherms corresponding to the nonacid CECs, while region 2 groups those of SA and CA. Overall, the adsorption data suggest that the interactions between the material and the CECs increases as follows: SA < CA < PXN < o-DMN  $< CFN < NPX < CBZ \le Ep$ -CBZ. The stronger interactions of the adsorbent with Ep-CBZ and CBZ, respectively, are plausibly due to the hydrophobic character of both CECs and that repulsion forces are not produced because, according to  $pK_a$ , both adsorbates would remain without charge at neutral pH conditions. The affinity toward NPX and CFN surpasses that toward the corresponding metabolites because the presence of methyl groups in the latter generates a reduction electronegativity. The low affinity toward SA and CA could be explained by the deprotonation of the molecules at neutral pH conditions (see p $K_a$  value in Table 1) and repulsion forces generated by the negatively charged surface. In the case of NPX and o-DMN, a hydrophobic behavior dominates the interactions, but unlike CBZ or Ep-CBZ, the deprotonation of these adsorbates produces repulsion forces with the AC-AT.

Data for single-component CEC adsorption onto CMOF (Figure 6C) indicate that interactions increase as follows: CA < SA <  $\sigma$ -DMN < PXN < NPX < CFN < Ep-CBZ < CBZ. An improvement in the adsorbed amounts of CECs compared to MOF was observed. The average adsorption loadings in region 1 between liquid phase concentrations of 1 and 1000  $\mu$ g L<sup>-1</sup> were 0.50 and 0.91 mg cm<sup>-3</sup> for MIL-100(Fe) and CMOF,

respectively. Also, the latter adsorbent exhibits substantial affinity toward all the nonacid CECs as a whole, with emphasis on CBZ, compared to the individual MOF and AC-AT. These are vastly due to the presence of the carbon on the composite, which effectively serves functions as a barrier to inhibit water interaction with the MOF and this also allows for the arise of specific interactions between the CECs and the MOF surface. Transition metals (i.e., Fe) serve as centers that attract adsorbates through various mechanisms, including  $\pi$ -complexation and  $\pi$ - $\pi$  stacking interactions. However, these centers are also prone to water agglomeration that may block accessibility of guest molecules (i.e., CEC) to the voids and, therefore, may hinder the aforementioned interactions. The CMOF may provide a way to circumvent this.

The affinity of CMOF toward CBZ and Ep-CBZ over NPX and o-DMN (adsorbates with larger log  $K_{\rm ow}$ ) could also be explained because, unlike the latter adsorbates group, CBZ and Ep-CBZ remain without electrostatic charge (see  $pK_a$  value in Table 1) and surface repulsion forces have little effect on them. The larger adsorbed amounts of the primary molecules over their corresponding metabolites could also be elucidated by the effect produced by their electronegativity and smaller molecular footprint. Furthermore, the lesser hydrophilic character of CFN compared to that of PXN contribute to better adsorbent—adsorbate interactions.

Figure 7 shows uptake equilibrium data (single component) for CBZ and NPX and several adsorbent materials, including

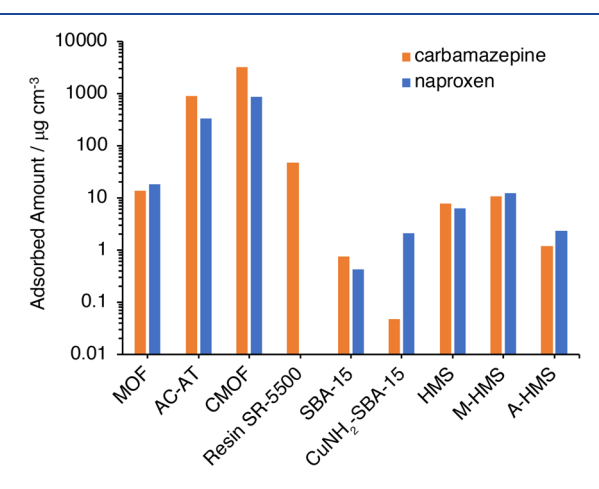


Figure 7. Single component uptake amounts for carbamazepine or naproxen adsorption ( $C_{\rm e} \sim 20~\mu {\rm g~L^{-1}}$ ) onto MIL-100(Fe) (MOF), activated carbon after acid treatment (AC-AT), MIL-100(Fe)/activated carbon composite (CMOF), polymeric resin SR-550, mesoporous silica SBA-15,  $^{34,53}$  copper-amine-functionalized mesoporous silica SBA-15 (CuNH<sub>2</sub>-SBA-15),  $^{34,53}$  hexagonal mesoporous silica (HMS),  $^{69}$  mercapto-functionalized HMS (M-HMS), or amine-functionalized HMS (A-HMS).

the ones considered in this study. For literature uptake data ranges of other CECs please refer to Table S3. All the data that were considered here were from reports where the aqueous phase concentration of the CEC was in the  $\mu g L^{-1}$  range. The materials considered for comparison purposes include a polymeric resin, mesoporous SBA-15, and hexagonal mesoporous silicas (HMS). In general, the CMOF adsorbent is capable of adsorbing CBZ and NPX, both bulky molecules, in amounts that are an order of magnitude larger than that of the resin and the silica ( $C_e = \sim 20 \ \mu g L^{-1}$ ).

To better visualize the synergistic effect of combining MIL-100(Fe) and activated carbon (as a composite) on the uptake of CECs, one could analyze the observe adsorption amounts on a per MOF unit cell basis. Using TGA (Figure 4) and the adsorbents textural properties (Table 2), the amount of MOF grown inside the pores of the AC accounted for about 46 wt % of the composite. Use of this datum to normalize the CECs single component adsorption amounts shown in Figure 6 translates to an average of  $6.9 \times 10^{-3}$  CEC molecules adsorbed per MOF unit cell in the case of the CMOF and about  $1.07 \times 10^{-3}$  CEC molecules adsorbed per MOF unit cell in the case of the as-prepared MOF, or approximately 10-fold more CEC molecules adsorbed in CMOF compared to the MOF.

**3.4.** Multicomponent CEC Equilibrium Adsorption. Multicomponent CEC adsorption isotherms are collected in Figure 6D–F. The presence of a matrix containing multiple CECs promotes competition between them for adsorption sites. This is quite evident in the case of the MIL-100(Fe) adsorbent (Figure 6D), where the compacting and overlapping of regions 1 and 2 are significant. The adsorption average capacity (accounting for both regions) was reduced by 31% when compared to the single-component data (i.e., Figure 6A). In the case of the AC-AT adsorbent, the competition affected mostly the overall capacity, which was reduced by 33% in region 1 compared to the single-component adsorption capacity (see also Figure S5).

In the case of CMOF, the effect of competition among the CECs on the adsorption capacity was not as significant. The average adsorption capacity circumscribed by region 1 is only 9% smaller compared to the case of single component adsorption. Furthermore, the capacity is 22% larger in region 1 when compared to that of AC-AT. Figure 6F also shows that the perimeter of region 1 is more compact compared to the one shown in Figure 6C, which could be due to the competition between CECs for adsorption sites, particularly those related to  $\pi$ -complexion and  $\pi$ - $\pi$  stacking.

**3.5. Recyclability Tests.** Figure 8 shows the percent of removal of carbamazepine in each cycle of adsorption. The

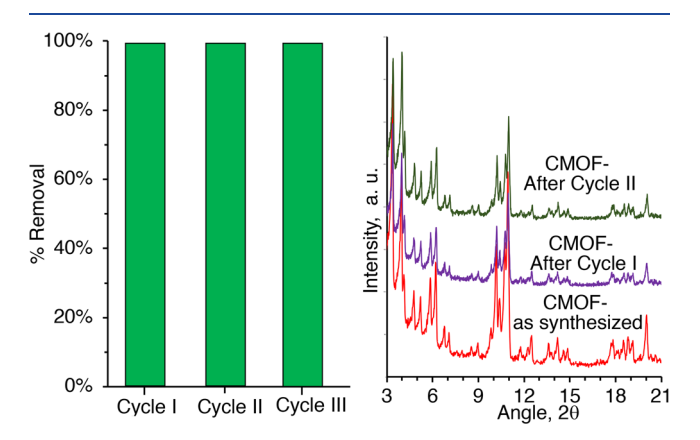


**Figure 8.** (Left) Percent of removal of carbamazepine with CMOF for each adsorption cycle. (Right) XRD pattern of CMOF adsorbent prior to the cycle of adsorption.

results show that efficiency remains constant (100%) even up to a third cycle of adsorption. Additionally, XRD profiles showed that a crystalline phase is still present in CMOF after adsorption cycles. This suggests that is plausible to desorb/decomposed carbamazepine from within the CMOF spent

adsorbent and recover the adsorbent without much detriment to the long-range properties.

#### 4. CONCLUSIONS

A composite nanoporous adsorbent material, CMOF, based on MIL-100(Fe) and activated carbon was successfully synthesized and characterized. Analysis of the textural properties as well as the long-range order of the periodic phase revealed the MOF crystals were grown inside the mesoporous cavities of the activated carbon, which is critical to ensure that the latter will offer hydrophobic abilities to the composite. Zeta potential measurements showed that nitric and hydrofluoric acids, reagents in the MIL-100Fe (MOF) synthesis, affected the surface of activated carbon, transferring negative electrostatic charge on the CMOF surface. However, the overall textural properties of the activated carbon portion of the composite were not affected probably because of protection by the MOF crystals. The CMOF adsorbent was also tested for the adsorption of CECs reported with high occurrence in water bodies. These tests were performed for CEC aqueous phase equilibrium concentrations in the  $\mu$ g L<sup>-1</sup> range and in singleand multicomponent fashion. The results showed that CMOF offers better adsorbent-adsorbate interactions in multicomponent tests, probably due to synergy from individual contributions that are characteristic of both primitive materials, MIL-100(Fe) and activated carbon. The hydrophobicity behavior of activated carbon limits water agglomeration around the transition metal node of the MOF structure and allows for better interactions with organic compounds; therefore, capacity and selectivity toward CECs in the multicomponent matrix is greater than that of the AC alone, even at low concentrations (i.e.,  $\mu g L^{-1}$ ). Compared to other adsorbents such as polymeric resins and silicas, the CMOF CEC adsorption amounts can be up to an order larger. The recyclability of CMOF was corroborated during three cycle adsorption/regeneration tests based on carbamazepine uptake.

#### ASSOCIATED CONTENT

# Supporting Information

The Supporting Information is available free of charge at https://pubs.acs.org/doi/10.1021/acsanm.0c00190.

Diffusion phenomenological model for the calculation of diffusion coefficient, parameters, and fitting plots for Sips and Freundlich models; estimated adsorption saturation values of CECs on adsorbents studied; average adsorbed amount for adsorbents reported elsewhere; time dependence adsorption; nitrogen adsorption—desorption isotherms gathered at  $-196~^{\circ}\text{C}$ ; TGA under air atmosphere; XPS spectra; and comparison of the adsorption capacity in single- and multicomponent materials studied (PDF)

#### AUTHOR INFORMATION

#### **Corresponding Author**

Arturo J. Hernández-Maldonado — Department of Chemical Engineering, University of Puerto Rico, Mayagüez, Puerto Rico 00681-9000; orcid.org/0000-0001-9379-8987;

Phone: 787-832-4040 ext. 3748; Email: arturoj.hernandez@upr.edu; Fax: 787-834-3655

#### **Authors**

- Juan C. Muñoz-Senmache Department of Chemical Engineering, University of Puerto Rico, Mayagüez, Puerto Rico 00681-9000
- Sewoon Kim Department of Civil and Environmental Engineering, University of South Carolina, Columbia, South Carolina 29208, United States
- Rodinson R. Arrieta-Pérez Department of Chemical Engineering, University of Puerto Rico, Mayagüez, Puerto Rico 00681-9000
- Chang Min Park Department of Environmental Engineering, Kyungpook National University, Daegu 41566, Republic of Korea; ⊚ orcid.org/0000-0003-0541-0300
- Yeomin Yoon Department of Civil and Environmental Engineering, University of South Carolina, Columbia, South Carolina 29208, United States; ⊙ orcid.org/0000-0001-9893-0924

Complete contact information is available at: https://pubs.acs.org/10.1021/acsanm.0c00190

# **Notes**

The authors declare no competing financial interest.

#### ACKNOWLEDGMENTS

Support for this project was provided by the National Science Foundation (NSF) under Grant No. OIA-1632824.

#### REFERENCES

- (1) Azadi, H.; Keramati, P.; Taheri, F.; Rafiaani, P.; Teklemariam, D.; Gebrehiwot, K.; Hosseininia, G.; Van Passel, S.; Lebailly, P.; Witlox, F. Agricultural land conversion: Reviewing drought impacts and coping strategies. *Int. J. Disaster Risk Reduct.* **2018**, 31, 184–195. (2) Mera, G. A. Drought and its impacts in Ethiopia. *Weather Clim.*
- (2) Mera, G. A. Drought and its impacts in Ethiopia. Weather Clim. Extrem. 2018, 22, 24–35.
- (3) Shrum, T. R.; Travis, W. R.; Williams, T. M.; Lih, E. Managing climate risks on the ranch with limited drought information. *Clim. Risk Manag.* **2018**, *20*, 11–26.
- (4) Drewes, J. E.; Anderson, P.; Denslow, N.; Jakubowski, W.; Olivieri, A.; Schlenk, D.; Snyder, S. Monitoring Strategies for Constituents of Emerging Concern (CECs) in Recycled Water: Recommendations of a Science Advisory Panel; Southern California Coastal Water Research Project Technical Report 1032, 2018.
- (5) Petrie, B.; Barden, R.; Kasprzyk-Hordern, B. A review on emerging contaminants in wastewaters and the environment: Current knowledge, understudied areas and recommendations for future monitoring. *Water Res.* **2015**, *72*, 3–27.
- (6) Glassmeyer, S. T.; Furlong, E. T.; Kolpin, D. W.; Batt, A. L.; Benson, R.; Boone, J. S.; Conerly, O.; Donohue, M. J.; King, D. N.; Kostich, M. S.; Mash, H. E.; Pfaller, S. L.; Schenck, K. M.; Simmons, J. E.; Varughese, E. A.; Vesper, S. J.; Villegas, E. N.; Wilson, V. S. Nationwide reconnaissance of contaminants of emerging concern in source and treated drinking waters of the United States. *Sci. Total Environ.* **2017**, *581–582*, 909–922.
- (7) Montes-Grajales, D.; Fennix-Agudelo, M.; Miranda-Castro, W. Occurrence of personal care products as emerging chemicals of concern in water resources: A review. *Sci. Total Environ.* **2017**, *595*, 601–614.
- (8) Yang, Y.; Ok, Y. S.; Kim, K.-H.; Kwon, E. E.; Tsang, Y. F. Occurrences and removal of pharmaceuticals and personal care products (PPCPs) in drinking water and water/sewage treatment plants: A review. *Sci. Total Environ.* **2017**, *596–597*, 303–320.
- (9) Al-Farsi, R. S.; Ahmed, M.; Al-Busaidi, A.; Choudri, B. S. Translocation of pharmaceuticals and personal care products (PPCPs) into plant tissues: A review. *Emerg. Contam.* **2017**, 3 (4), 132–137.

- (10) Ben Mordechay, E.; Tarchitzky, J.; Chen, Y.; Shenker, M.; Chefetz, B. Composted biosolids and treated wastewater as sources of pharmaceuticals and personal care products for plant uptake: A case study with carbamazepine. *Environ. Pollut.* **2018**, 232, 164–172.
- (11) Madikizela, L. M.; Ncube, S.; Chimuka, L. Uptake of pharmaceuticals by plants grown under hydroponic conditions and natural occurring plant species: A review. *Sci. Total Environ.* **2018**, 636, 477–486.
- (12) Pullagurala, V. L. R.; Rawat, S.; Adisa, I. O.; Hernandez-Viezcas, J. A.; Peralta-Videa, J. R.; Gardea-Torresdey, J. L. Plant uptake and translocation of contaminants of emerging concern in soil. *Sci. Total Environ.* **2018**, *636*, 1585–1596.
- (13) Pedrazzani, R.; Bertanza, G.; Brnardić, I.; Cetecioglu, Z.; Dries, J.; Dvarionienė, J.; García-Fernández, A. J.; Langenhoff, A.; Libralato, G.; Lofrano, G.; Škrbić, B.; Martínez-López, E.; Meriç, S.; Pavlović, D. M.; Papa, M.; Schröder, P.; Tsagarakis, K. P.; Vogelsang, C. Opinion paper about organic trace pollutants in wastewater: Toxicity assessment in a European perspective. *Sci. Total Environ.* **2019**, *651*, 3202–3221.
- (14) Prosser, R. S.; Sibley, P. K. Human health risk assessment of pharmaceuticals and personal care products in plant tissue due to biosolids and manure amendments, and wastewater irrigation. *Environ. Int.* **2015**, *75*, 223–233.
- (15) Gwenzi, W.; Chaukura, N. Organic contaminants in African aquatic systems: Current knowledge, health risks, and future research directions. *Sci. Total Environ.* **2018**, *619–620*, 1493–1514.
- (16) Eggen, R. I. L.; Hollender, J.; Joss, A.; Scharer, M.; Stamm, C. Reducing the discharge of micropollutants in the aquatic environment: The benefits of upgrading wastewater treatment plants. *Environ. Sci. Technol.* **2014**, 48 (14), 7683–7689.
- (17) Rizzo, L.; Malato, S.; Antakyali, D.; Beretsou, V. G.; Đolic, M. B.; Gernjak, W.; Heath, E.; Ivancev-Tumbas, I.; Karaolia, P.; Lado Ribeiro, A. R.; Mascolo, G.; McArdell, C. S.; Schaar, H.; Silva, A. M.T.; Fatta-Kassinos, D. Consolidated vs new advanced treatment methods for the removal of contaminants of emerging concern from urban wastewater. *Sci. Total Environ.* **2019**, *655*, 986–1008.
- (18) Patel, M.; Kumar, R.; Kishor, K.; Mlsna, T.; Pittman, C. U.; Mohan, D. Pharmaceuticals of emerging concern in aquatic systems: chemistry, occurrence, effects, and removal methods. *Chem. Rev.* **2019**, *119* (6), 3510–3673.
- (19) Wang, J.; Chu, L. Irradiation treatment of pharmaceutical and personal care products (PPCPs) in water and wastewater: An overview. *Radiat. Phys. Chem.* **2016**, 125, 56–64.
- (20) Kim, S.; Chu, K. H.; Al-Hamadani, Y. A. J.; Park, C. M.; Jang, M.; Kim, D.-H.; Yu, M.; Heo, J.; Yoon, Y. Removal of contaminants of emerging concern by membranes in water and wastewater: A review. *Chem. Eng. J.* **2018**, 335, 896–914.
- (21) Goswami, L.; Vinoth Kumar, R.; Borah, S. N.; Arul Manikandan, N.; Pakshirajan, K.; Pugazhenthi, G. Membrane bioreactor and integrated membrane bioreactor systems for micropollutant removal from wastewater: A review. *J. Water Process Eng.* **2018**, *26*, 314–328.
- (22) Basheer, A. New generation nano-adsorbents for the removal of emerging contaminants in water. *J. Mol. Liq.* **2018**, 261, 583–593.
- (23) Gao, Q.; Xu, J.; Bu, X.-H. Recent advances about metal-organic frameworks in the removal of pollutants from wastewater. *Coord. Chem. Rev.* **2019**, *378*, 17–31.
- (24) Joseph, L.; Jun, B.-M.; Jang, M.; Park, C. M.; Muñoz-Senmache, J. C.; Hernández-Maldonado, A. J.; Heyden, A.; Yu, M.; Yoon, Y. Removal of contaminants of emerging concern by metal-organic framework nanoadsorbents: A review. *Chem. Eng. J.* **2019**, *369*, 928–946.
- (25) Ahmed, M. J. Adsorption of non-steroidal anti-inflammatory drugs from aqueous solution using activated carbons: Review. *J. Environ. Manage.* **2017**, *190*, 274–282.
- (26) Indherjith, S.; Karthikeyan, S.; Monica, J. H. R.; Krishna Kumar, K. Graphene oxide & reduced graphene oxide polysulfone nanocomposite pellets: An alternative adsorbent of antibiotic pollutant-ciprofloxacin. *Sep. Sci. Technol.* **2019**, *54* (5), 667–674.

- (27) Pamphile, N.; Xuejiao, L.; Guangwei, Y.; Yin, W. Synthesis of a novel core-shell-structure activated carbon material and its application in sulfamethoxazole adsorption. *J. Hazard. Mater.* **2019**, *368*, 602–612.
- (28) Zhao, C. Q.; Hong, P. D.; Li, Y. J.; Song, X. M.; Wang, Y. G.; Yang, Y. S. Mechanism of adsorption of tetracycline-Cu multipollutants by graphene oxide (GO) and reduced graphene oxide (rGO). J. Chem. Technol. Biotechnol. 2018, 94 (4), 1176–1186.
- (29) González-Ramos, K. M.; Fernández-Reyes, B.; Román, F. R.; Hernández-Maldonado, A. J. A hierarchical porous carbon M<sup>n+</sup>[FAU] (M<sup>n+</sup>=Ni<sup>2+</sup> or Cu<sup>2+</sup>) adsorbent: Synthesis, characterization and adsorption of salicylic acid from water. *Microporous Mesoporous Mater.* **2014**, 200, 225–234.
- (30) de Sousa, D. N. R.; Insa, S.; Mozeto, A. A.; Petrovic, M.; Chaves, T. F.; Fadini, P. S. Equilibrium and kinetic studies of the adsorption of antibiotics from aqueous solutions onto powdered zeolites. *Chemosphere* **2018**, 205, 137–146.
- (31) Jiang, N.; Shang, R.; Heijman, S. G. J.; Rietveld, L. C. High-silica zeolites for adsorption of organic micro-pollutants in water treatment: A review. *Water Res.* **2018**, *144*, 145–161.
- (32) Li, Z. C.; Gomez-Aviles, A.; Sellaoui, L.; Bedia, J.; Bonilla-Petriciolet, A.; Belver, C. Adsorption of ibuprofen on organo-sepiolite and on zeolite/sepiolite heterostructure: Synthesis, characterization and statistical physics modeling. *Chem. Eng. J.* **2019**, *371*, 868–875.
- (33) Oliveira, M. F.; de Souza, V. M.; da Silva, M. G. C.; Vieira, M. G. A. Fixed-bed adsorption of caffeine onto thermally modified verdelodo bentonite. *Ind. Eng. Chem. Res.* **2018**, *57* (51), 17480–17487.
- (34) Ortiz-Martínez, K.; Vargas-Valentín, D. A.; Hernández-Maldonado, A. J. Adsorption of contaminants of emerging concern from aqueous solutions using Cu<sup>2+</sup> amino grafted SBA-15 mesoporous silica: multicomponent and metabolites adsorption. *Ind. Eng. Chem. Res.* **2018**, 57 (18), 6426–6439.
- (35) Barczak, M. Amine-modified mesoporous silicas: Morphology-controlled synthesis toward efficient removal of pharmaceuticals. *Microporous Mesoporous Mater.* **2019**, 278, 354–365.
- (36) Choi, Y.; Sinha, A.; Im, J.; Jung, H.; Kim, J. Hierarchically porous composite scaffold composed of SBA-15 microrods and reduced graphene oxide functionalized with cyclodextrin for water purification. ACS Appl. Mater. Interfaces 2019, 11 (17), 15764–15772.
- (37) Khan, N. A.; Jung, B. K.; Hasan, Z.; Jhung, S. H. Adsorption and removal of phthalic acid and diethyl phthalate from water with zeolitic imidazolate and metal-organic frameworks. *J. Hazard. Mater.* **2015**, 282, 194–200.
- (38) Hasan, Z.; Khan, N. A.; Jhung, S. H. Adsorptive removal of diclofenac sodium from water with Zr-based metal-organic frameworks. *Chem. Eng. J.* **2016**, 284, 1406–1413.
- (39) Azhar, M. R.; Abid, H. R.; Periasamy, V.; Sun, H. Q.; Tade, M. O.; Wang, S. B. Adsorptive removal of antibiotic sulfonamide by UiO-66 and ZIF-67 for wastewater treatment. *J. Colloid Interface Sci.* **2017**, 500, 88–95.
- (40) Wang, J.; Wang, S. Removal of pharmaceuticals and personal care products (PPCPs) from wastewater: A review. *J. Environ. Manage.* **2016**, *182*, 620–640.
- (41) Yaghi, O. M.; O'Keeffe, M.; Ockwig, N. W.; Chae, H. K.; Eddaoudi, M.; Kim, J. Reticular synthesis and the design of new materials. *Nature* **2003**, 423, 705–714.
- (42) Hasan, Z.; Choi, E.-J.; Jhung, S. H. Adsorption of naproxen and clofibric acid over a metal-organic framework MIL-101 functionalized with acidic and basic groups. *Chem. Eng. J.* **2013**, 219, 537–544.
- (43) Huo, S.-H.; Yan, X.-P. Metal-organic framework MIL-100(Fe) for the adsorption of malachite green from aqueous solution. *J. Mater. Chem.* **2012**, 22 (15), 7449–7455.
- (44) Cai, J. H.; Mao, X. H.; Song, W. G. Adsorption behavior and structure transformation of mesoporous metal-organic frameworks towards arsenates and organic pollutants in aqueous solution. *Mater. Chem. Front.* **2018**, 2 (7), 1389–1396.
- (45) Georgiou, Y.; Perman, J. A.; Bourlinos, A. B.; Deligiannakis, Y. Highly efficient arsenite As(III) adsorption by an MIL-100(Fe) metal-

- organic framework: Structural and mechanistic insights. *J. Phys. Chem.* C 2018, 122 (9), 4859–4869.
- (46) Han, L. J.; Ge, F. Y.; Sun, G. H.; Gao, X. J.; Zheng, H. G. Effective adsorption of Congo red by a MOF-based magnetic material. *Dalton Trans.* **2019**, *48* (14), 4650–4656.
- (47) Nehra, M.; Dilbaghi, N.; Singhal, N. K.; Hassan, A. A.; Kim, K. H.; Kumar, S. Metal organic frameworks MIL-100(Fe) as an efficient adsorptive material for phosphate management. *Environ. Res.* **2019**, 169, 229–236.
- (48) Horcajada, P.; Surble, S.; Serre, C.; Hong, D.-Y.; Seo, Y.-K.; Chang, J.-S.; Greneche, J.-M.; Margiolaki, I.; Ferey, G. Synthesis and catalytic properties of MIL-100(Fe), an iron(III) carboxylate with large pores. *Chem. Commun.* **2007**, No. 27, 2820–2822.
- (49) Yoon, J. W.; Seo, Y.-K.; Hwang, Y. K.; Chang, J.-S.; Leclerc, H.; Wuttke, S.; Bazin, P.; Vimont, A.; Daturi, M.; Bloch, E.; Llewellyn, P. L.; Serre, C.; Horcajada, P.; Greneche, J.-M.; Rodrigues, A. E.; Ferey, G. Controlled reducibility of a metal-organic framework with coordinatively unsaturated sites for preferential gas sorption. *Angew. Chem., Int. Ed.* **2010**, 49 (34), 5949–5952.
- (50) Seo, Y.-K.; Yoon, J. W.; Lee, J. S.; Lee, U. H.; Hwang, Y. K.; Jun, C.-H.; Horcajada, P.; Serre, C.; Chang, J.-S. Large scale fluorine-free synthesis of hierarchically porous iron(III) trimesate MIL-100(Fe) with a zeolite MTN topology. *Microporous Mesoporous Mater.* **2012**, *157*, 137–145.
- (51) Seo, Y.-K.; Yoon, J. W.; Lee, J. S.; Hwang, Y. K.; Jun, C.-H.; Chang, J.-S.; Wuttke, S.; Bazin, P.; Vimont, A.; Daturi, M.; Bourrelly, S.; Llewellyn, P. L.; Horcajada, P.; Serre, C.; Ferey, G. Energy-Efficient Dehumidification over Hierachically Porous Metal-Organic Frameworks as Advanced Water Adsorbents. *Adv. Mater.* **2012**, *24* (6), 806–810.
- (52) Rivera-Jiménez, S. M.; Méndez-González, S.; Hernández-Maldonado, A. Metal (M = Co<sup>2+</sup>, Ni<sup>2+</sup>, and Cu<sup>2+</sup>) grafted mesoporous SBA-15: Effect of transition metal incorporation and pH conditions on the adsorption of Naproxen from water. *Microporous Mesoporous Mater.* **2010**, 132 (3), 470–479.
- (53) Ortiz-Martínez, K.; Guerrero-Medina, K. J.; Román, F. R.; Hernández-Maldonado, A. J. Transition metal modified mesoporous silica adsorbents with zero microporosity for the adsorption of contaminants of emerging concern (CECs) from aqueous solutions. *Chem. Eng. J.* 2015, 264, 152–164.
- (54) Bezverkhyy, I.; Weber, G.; Bellat, J. P. Degradation of fluoride-free MIL-100(Fe) and MIL-53(Fe) in water: Effect of temperature and pH. *Microporous Mesoporous Mater.* **2016**, 219, 117–124.
- (55) Fernández-Catalá, J.; Casco, M. E.; Martínez-Escandell, M.; Rodríguez-Reinoso, F.; Silvestre-Albero, J. HKUST-1@ACM hybrids for adsorption applications: A systematic study of the synthesis conditions. *Microporous Mesoporous Mater.* **2017**, 237, 74–81.
- (56) Brunauer, S.; Emmett, P. H.; Teller, E. Adsorption of Gases in Multimolecular Layers. J. Am. Chem. Soc. 1938, 60 (2), 309–319.
- (57) Barrett, E. P.; Joyner, L. G.; Halenda, P. P. The Determination of Pore Volume and Area Distributions in Porous Substances. I. Computations from Nitrogen Isotherms. *J. Am. Chem. Soc.* **1951**, 73 (1), 373–380.
- (58) Rege, S. U.; Yang, R. T. Corrected Horváth-Kawazoe equations for pore-size distribution. *AIChE J.* **2000**, *46* (4), 734–750.
- (59) Carballa, M.; Omil, F.; Lema, J. M. Removal of cosmetic ingredients and pharmaceuticals in sewage primary treatment. *Water Res.* **2005**, 39 (19), 4790–4796.
- (60) Said, S. A. M.; Qadir, N. U.; Mansour, R. B.; Mezghani, K.; Irshad, H. M. Synthesis and water sorption properties of a series of exfoliated graphene/MIL-100(Fe) composites. *RSC Adv.* **2017**, 7 (28), 17353–17356.
- (61) Patra, S.; Hidalgo Crespo, T.; Permyakova, A.; Sicard, C.; Serre, C.; Chaussé, A.; Steunou, N.; Legrand, L. Design of metal organic framework-enzyme based bioelectrodes as a novel and highly sensitive biosensing platform. *J. Mater. Chem. B* **2015**, *3* (46), 8983–8992.
- (62) Cortés-Súarez, J.; Celis-Arias, V.; Beltrán, H. I.; Tejeda-Cruz, A.; Ibarra, I. A.; Romero-Ibarra, J. E.; Sánchez-González, E.; Loera-Serna, S. Synthesis and Characterization of an SWCNT@HKUST-1

- Composite: Enhancing the CO2 Adsorption Properties of HKUST-1. ACS Omega 2019, 4 (3), 5275-5282.
- (63) Fleker, O.; Borenstein, A.; Lavi, R.; Benisvy, L.; Ruthstein, S.; Aurbach, D. Preparation and properties of metal organic framework/activated carbon composite materials. *Langmuir* **2016**, 32 (19), 4935–4944.
- (64) Lv, H.; Zhao, H.; Cao, T.; Qian, L.; Wang, Y.; Zhao, G. Efficient degradation of high concentration azo-dye wastewater byheterogeneous Fenton process with iron-based metal-organicframework. J. Mol. Catal. A: Chem. 2015, 400, 81–89.
- (65) Lemraski, E. G.; Sharafinia, S. Kinetics, equilibrium and thermodynamics studies of Pb2+ adsorption onto new activated carbon prepared from Persian mesquite grain. *J. Mol. Liq.* **2016**, *219*, 482–492.
- (66) Zhu, B.-J.; Yu, X.-Y.; Jia, Y.; Peng, F.-M.; Sun, B.; Zhang, M.-Y.; Luo, T.; Liu, J.-H.; Huang, X.-J. Iron and 1,3,5-Benzenetricarboxylic Metal-Organic Coordination Polymers Prepared by Solvothermal Method and Their Application in Efficient As(V) Removal from Aqueous Solutions. *J. Phys. Chem. C* **2012**, *116* (15), 8601–8607.
- (67) Hasan, Z.; Jhung, S. H. Removal of hazardous organics from water using metal-organic frameworks (MOFs): Plausible mechanisms for selective adsorptions. *J. Hazard. Mater.* **2015**, 283, 329–339.
- (68) Khan, N. A.; Jhung, S. H. Adsorptive removal and separation of chemicals with metal-organic frameworks: Contribution of  $\pi$ -complexation. *J. Hazard. Mater.* **2017**, 325, 198–213.
- (69) Suriyanon, N.; Permrungruang, J.; Kaosaiphun, J.; Wongrueng, A.; Ngamcharussrivichai, C.; Punyapalakul, P. Selective adsorption mechanisms of antilipidemic and non-steroidal anti-inflammatory drug residues on functionalized silica-based porous materials in a mixed solute. *Chemosphere* **2015**, *136*, 222–231.
- (70) Haddad, M.; Oie, C.; Vo Duy, S.; Sauve, S.; Barbeau, B. Adsorption of micropollutants present in surface waters onto polymeric resins: Impact of resin type and water matrix on performance. *Sci. Total Environ.* **2019**, *660*, 1449–1458.